Thermo-temporal physisorption in metal–organic frameworks probed by cyclic thermo-ellipsometry

Hajar Amyar, Civan Avci, Cédric Boissière, Andrea Cattoni, Mondher Besbes,
Marco Faustini

HAL Id: hal-04746163

https://hal.sorbonne-universite.fr/hal-04746163v1

Submitted on 21 Oct 2024

ChemComm

COMMUNICATION

Thermo-temporal Physisorption in Metal-Organic Frameworks probed by Cyclic Thermo-Ellipsometry

Hajar Amyar,[a] Civan Avci,[a] Cédric Boissière,[a] Andrea Cattoni,[b,c] Mondher Besbes[d] and Marco Faustini*[a,e]

Temperature-induced sorption in porous materials is a well-known process. What is more challenging is to determine how the rate at which temperature is varied affects these processes. To address this question, we introduce a methodology called "cyclic thermo-ellipsometry" to explore the thermo-kinetics of vapor physisorption in Metal-Organic Framework films.

[a] Sorbonne Université, CNRS, Laboratoire Chimie de la Matière Condensée de Paris (LCMCP), F-75005 Paris, France
[b] Centre de Nanosciences et de Nanotechnologies (C2N), CNRS UMR 9001, Université Paris-Saclay, Palaiseau, France.
[c] Dipartimento di Fisica, Politecnico di Milano, Via Giuseppe Colombo, Milano 20133, Italy
[d] Université Paris-Saclay, Institut d'Optique Graduate School, CNRS, Laboratoire Charles Fabry, 91127 Palaiseau, France
[e] Institut Universitaire de France (IUF), 75231 Paris, France
Electronic Supplementary Information (ESI) available See DOI: 10.1039/x0xx00000x

Adsorption-driven heat transformation,[1] water harvesting,[2] cooling of electronic devices[3] and temperature sensing[4] are all key technologies that utilize adsorption and desorption of vapors into and from porous materials, driven by temperature changes. Metal-Organic Frameworks (MOFs) are considered among the best candidates for various adsorption-driven applications. For example, MOFs can be used as water-based adsorption-driven chillers or heat pumps; these rely on reversible multi-cycling adsorption-desorption of water vapor, with material regeneration after each cycle achieved through heating. MOFs have been used for atmospheric water harvesting to capture water from the air and releasing it by solar heating. Thermal-driven sorption also has high significance in the context of direct air capture of CO_2 and regeneration of sorbent materials.[5] For all this applications, benchmarking sorption performances, cyclability and regeneration capabilities of MOFs requires probing their thermal kinetic response. Many methods can be used to probe the sorption capabilities close to the thermodynamic equilibrium; however, assessing the MOFs sorption response to dynamically changing conditions (e.g., large temperature changes) is not an easy task. There are different methods to probe adsorption kinetics in porous materials, depending on the specific properties of the material and the desired level of detail of the analysis. Gravimetric methods have been used to determine diffusion coefficient of analyte molecules into MOFs. For instance, diffusion kinetics of water or benzene in MIL-101 was evaluated from uptake/desorption relaxation curves.[6] This method requires a precise balance and can be time-consuming. Achieving abrupt and controlled changes of vapor pressure can be challenging with the set-up used for gravimetric experiments. In alternative, spectroscopic analyses such as infrared or Raman spectroscopy enable monitoring the adsorption of molecules in MOFs.[7] However they can suffer from a limited time resolution and/or from the fact that quantitative evaluation can require demanding calibrations. More generally, comparing kinetics of powder materials is challenging, since they suffer from limitation related to interparticle mass transport and thermal exchange, not negligible in case of very fast kinetics. Beyond powders, thin films can represent an appealing configuration where thermal exchanges are very fast, thereby reducing thermal and mass diffusion constraints. One powerful method to characterize films is spectroscopic ellipsometry. Equipped with environmental chambers, ellipsometry enables monitoring the evolution of refractive index $n(\lambda)$ of films vs time under controlled conditions.[8] Notably, the so-called "Environmental Ellipsometric Porosimetry" (EEP) is well suited to characterize the porosity through vapor physisorption.[9] EEP has been used to characterize MOF films and investigate the pore size distribution, pore volumes and, in some cases, mechanical properties.[10] However, these characterizations are usually
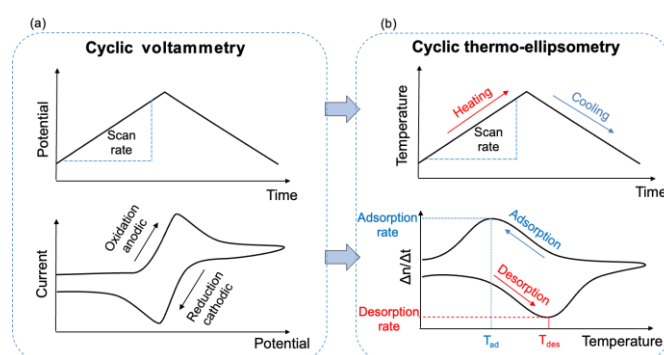

Figure 1 *Schematic representation of the analogy between cyclic voltammetry and cyclic thermo-ellipsometry to visualize thermo-adsorptive events.*

done "at equilibrium" and at constant temperature. In-situ ellipsometry was used to evaluate the vapor uptake kinetics in ZIF-8 based sensors leading to a kinetic selective response,[11] yet at constant temperature. Taking advantages of the versatility and temporal resolution (0.1s) of ellipsometric analysis, one could in principle design new experiments aiming at unveiling the thermo-temporal sorption and structural response of MOFs films in dynamically changing conditions. To do that, one needs to (i) design an experiment in which kinetic parameters can be obtained in a reliable way; (ii) find a convenient way to plot and analyse the dynamic data.

To do that, we took inspiration from electrochemistry and especially cyclic voltammetry (CV), a powerful method to describe electron transfer processes of molecular species.[12] In a CV experiment, the electrode potential ramps linearly versus time in cyclical phases (Figure 1a). The change of voltage over time is called scan rate (V/s). The outcome of the measurement is a current (*i*) versus applied potential (*E*). In presence of an oxidable specie, by increasing E, the anodic current will first increase, reaching a peak and some point after the oxidation potential of the analyte is reached, the current will decrease as the concentration of oxidable analyte is depleted. If the process is reversible, then during the reverse scan the oxidized analyte will start to be re-reduced, giving rise to a current of reverse polarity (cathodic current) to before. Several cycles at increasing scan rate can be performed providing information about redox potentials and electrochemical reaction rates. If we now draw the analogy with CV, in the so-called "cyclic thermo-ellipsometry" experiment in presence of vapor, the temperature can be increased and decreased linearly at a certain scan rate $\Delta T/\Delta t$ (Figure 1b) provoking the vapor molecules to be adsorbed or desorbed from the porous film. In this case, the temperature is the parameter to tune the chemical potential. This mass exchange can be detected by ellipsometry through the change in refractive index Δn. The derivative of the refractive index as respect to time $\Delta n/\Delta t$ can be seen as mass flow (by analogy with current) or sorption rate that is positive in case of adsorption and negative in case of desorption.
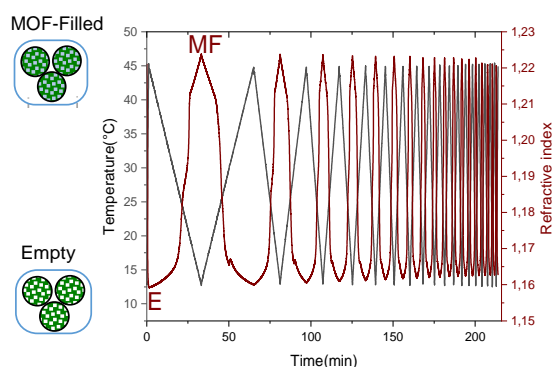
Figure 3 *Thermo-kinetic plot showing the evolution of the refractive index as function of time of MIL-101 films submitted to heating/cooling cycling at increasing scan rate.*

We customized a thermo-adsorptive ellipsometry set-up as illustrated in Figure 2a. The experiment is carried out in a closed chamber equipped with a programmable thermal stage enabling the substrate to be heated or cooled. In addition, we inject in the chamber a flow of air at 20°C containing a constant $P/P_0^{(20°C)}$ of water vapor generated by a mass flow controller and measured by humidity sensor before injection in the chamber. In this configuration, as illustrated in Figure S1, the substrate is heated and cooled while the surrounding atmosphere remains at 20°C as verified by a thermocouple. A temperature gradient between the atmosphere and the film is thus generated during the experiment. According to the Clausius-Clapeyron relation, increasing the temperature of the film results in a local increase of the saturation vapor pressure P_0. Since the vapor pressure P remains constant, a gradient of relative vapor pressure P/P_0 between the atmosphere and the film is obtained by changing the temperature of the film. In presence of a porous film we thus obtain adsorption and desorption isobars (constant pressure and variable temperature). As case of study we focused on MIL-101(Cr), a stable hydrophilic mesoporous MOF and one of the most promising sorbent for water-adsorption based applications;[13] beyond applications, due to its multimodal porosity, MIL-

101(Cr) represents an ideal model system to explore the capabilities of our approach. This porous material is made from hybrid supertetrahedra (ST) of chromium trimers connected through terephthalate linkers. The hybrid framework is composed by two types of mesoporous cages as illustrated in the Figure 2b: small mesoporous cages having free internal diameters of 2.9 nm and large cages of 3.4 nm in a 2 : 1 ratio connected by windows of ~1.17 and ~1.6 nm, respectively.[13] The colloidal MIL-101(Cr) was applied by spin-coating on a silicon wafer substrate. The SEM micrograph in Figure 2c displays a cross section view of a typical MIL-101(Cr) colloidal film composed of nanoparticles having average size of 50 nm (as evaluated by SEM micrographs) and a thickness of around 250nm (evaluated by ellipsometry). The crystallinity of the materials was first confirmed by X-ray diffraction (Figure S2). Figure 2d illustrates the isobars of the colloidal MIL-101(Cr) film in presence of a constant relative vapour pressure of H_2O = 0.5 $P/P_0^{(20°C)}$ and expressed as the evolution of refractive index (at 700nm) and thickness (Figure S3) as function of the temperature. On Figure 2d at T = 50°C, the colloidal film presents a low refractive index of 1.16 suggesting that the film is highly porous.[10b] At high temperature, almost no water molecules are adsorbed, the state is named "empty" (E).

Decreasing slowly the temperature (1°C min^{-1}) the local P/P_0 increases. At 24 and 21°C, two increases in refractive index are observed. These water adsorption steps correspond to two monodisperse pore sizes attributed to the large and small cages illustrated in Figure 2b as reported in previous findings[10b, 14]. After filling, the porosity of the MOF is filled (state "MF"). Further cooling leads to another increase of refractive index at 8-9°C attributed to the capillary condensation of water molecules in the mesopores formed by inter-particle voids of the film. This final state is named "Filled" (F). By heating back the material at 50°C, desorption occurs. Interestingly, the hysteresis loop between the state "MF" and "E" is attributed to the two windows acting as a restriction to water desorption from MIL-101(Cr). In this configuration, at
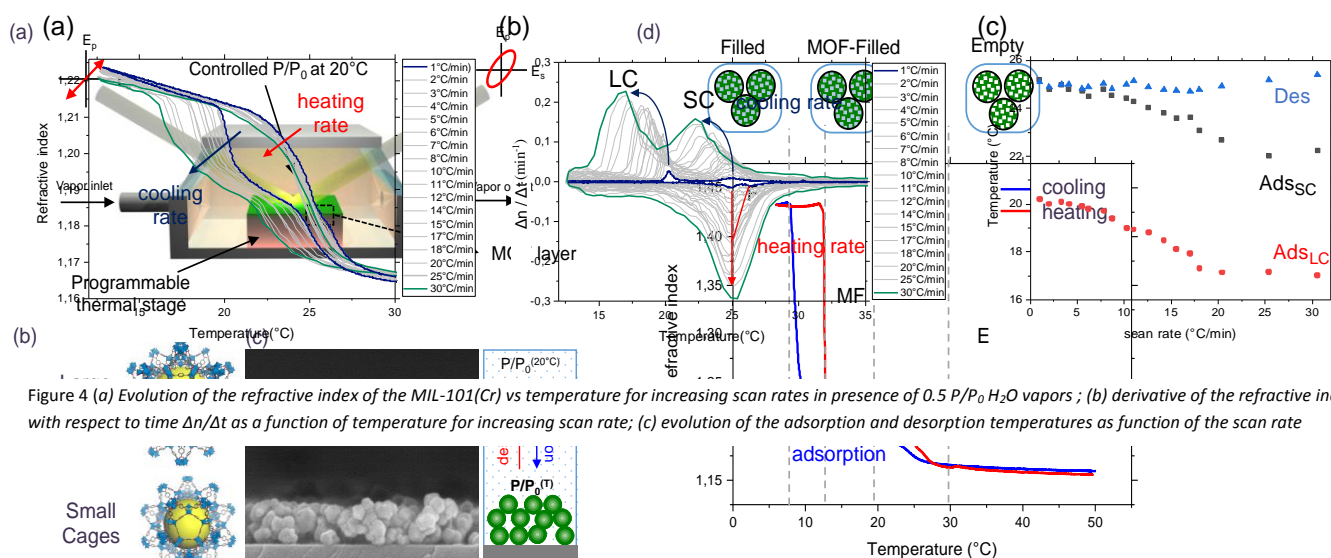

Figure 4 *(a) Evolution of the refractive index of the MIL-101(Cr) vs temperature for increasing scan rates in presence of 0.5 P/P_0 H_2O vapors ; (b) derivative of the refractive index with respect to time $\Delta n/\Delta t$ as a function of temperature for increasing scan rate; (c) evolution of the adsorption and desorption temperatures as function of the scan rate*

Figure 2 *(a) Illustration of the ellipsometric set-up (b) Illustration of large and small mesoporous cages in MIL-101(Cr) and (c) cross section SEM micrograph of the colloidal film, scale bar=200nm (d) Water isobar of a MIL-101(Cr) film performed at 0.5 P/P_0 and with a heating/cooling rate of 1°Cmin^{-1}*

COMMUNICATION   ChemComm

50°C the refractive index goes back to the initial value of 1.15, in contrast with experiments at constant temperature.[10b] This reversibility is also confirmed by the evolution of thickness as shown in Figure S3. By using the Bruggemann effective medium approximation (BEMA) model (SI),[15] we determined that the small cages, larges cages and interparticle mesoporosities represent around the 8%, 12% and 80% of the total porosity. In the example discussed above, the adsorption and desorption have been induced by heating and cooling with a relatively slow thermal ramp of 1°C min^{-1}. We then access the cyclability and the thermo-temporal response of the materials when the system is "pushed" out-of-equilibrium. To do so, we employed cycles of adsorption and desorption by increasing the scan rate up from 1 to 30°C min^{-1}. To study exclusively the contribution of the mesoporosity of the MIL-101(Cr) nanoparticles we analysed the temperature range between 12.5°C and 45°C corresponding to the transition between the "MF" and the "E" states.

Figure 3 shows the thermo-kinetic plots representing the evolution of the refractive index (red curve), as function of the time while applying temperature ramps at increasing speed (black lines). On a first sight, the temperature driven adsorption/desorption events are reversible and the material is cycling. Before going further in the analysis we challenged our experimental set-up in order to exclude possible artefacts. We first verified the reproducibility of the environmental set-up with different vapour pressure, samples and by modifying the temperature range and the acquisition times. Second, we confirmed the reliability of the heating stage, thermocouples and gas flow system to rule out a possible effect due to thermal inertia of the thermal plate or other time-delays (Figure S4). We then plot the isobars of refractive index as function of the temperature for each different scan rate Figure 4a. Interestingly, the curves do not overlap indicating a rate-dependency. As the scan rate increases, the hysteresis becomes wider from the blue curve to the green curve. We then further analysed the data by plotting the derivative of the refractive index with respect to time $\Delta n/\Delta t$ as a function of temperature for each scan rate, as shown in Figure 4b. Interestingly, the shape of the curves reminds the typical cyclic voltammograms. By this plot, the evolution of both adsorption and desorption for each cage/restriction can be monitored independently. Two peaks appear during adsorption that correspond to the contribution of the two mesopore sizes in the nanoparticle. At low scan rate, two peaks are visible during desorption probably corresponding to the two pore windows of ~1.17 and ~1.6 nm acting as restriction in MIL-101.[13] Interestingly, while at low scan rate (1°C min^{-1}, blue curve) the two desorption peaks are well separated suggesting two distinct desorption events separated in time, they partially overlap while increasing the scan rate. The adsorption peaks for both SC and LC cages shift toward lower temperatures increasing the scan rate. The evolution of the adsorption or desorption temperatures (position of the peak) as function of the scan rate is shown in Figure 4c. The analysis indicates that the desorption temperature doesn't vary with the scan rate; instead the adsorption temperature for both SC and LC shifts towards lower values increasing the cooling rate to reach a

shift of 3°C between 1 and 30°$Cmin^{-1}$. To generalize the approach, another similar study was carried out on microporous ZIF-8 colloidal films and isopropyl alcohol vapors (Figure S5, S6, and S7). It is well-known that microporous materials such as ZIF-8 should exhibit no hysteresis at thermodynamic equilibrium. However, by performing cyclic thermo-ellipsometry analysis on the microporosity of ZIF-8, both adsorption and desorption peaks shift toward lower and higher temperatures, respectively, showing a widening hysteresis with the scan rate. This strong rate-dependency suggests that under these conditions, the system is out of equilibrium. Explaining the effect temperature and temperature changes on vapor adsorption and desorption processes in MOFs is not straightforward and is beyond the scope of this work. Approaches based on simulation are usually required to the describe the uptake into complex porosity of MOFs with nonuniform pore surface properties.[16] [17] Nevertheless, the present methodology based on cyclic thermo-ellipsometry can provide key fundamental insights on thermotemporal sorption events that combined with simulation can enhanced our comprehension in these complex rate-dependent phenomena. From a more applied perspective, cyclic thermo-ellipsometry can emerge as a promising and convenient methodology to benchmark thermokinetic performances and cyclability of other porous materials beyond MOFs and for applications such as adsorption-driven chillers or heat pumps, water harvesting or even CO_2 capture.

Conflicts of interest

There are no conflicts to declare

Notes and references

1   (a) L. Garzón-Tovar, J. Pérez-Carvajal, I. Imaz and D. Maspoch, *Advanced Functional Materials*, 2017, **27**, 1606424; (b) G. Mouchaham, F. S. Cui, F. Nouar, V. Pimenta, J.-S. Chang and C. Serre, *Trends in chemistry*, 2020, **2**, 990; (c) A. Cadiau, J. S. Lee, D. Damasceno Borges, P. Fabry, T. Devic, M. T. Wharmby, C. Martineau, D. Foucher, F. Taulelle and C. H. Jun, *Advanced Materials*, 2015, **27**, 4775.

2   (a) A. LaPotin, H. Kim, S. R. Rao and E. N. Wang, *Accounts of Chemical Research*, 2019, **52**, 1588; (b)   N. Hanikel, X. Pei, S. Chheda, H. Lyu, W. Jeong, J. Sauer, L. Gagliardi and O. M. Yaghi, *Science*, 2021, **374**, 454.

3   C. Wang, L. Hua, H. Yan, B. Li, Y. Tu and R. Wang, *Joule*, 2020, **4**, 435.

4   (a) C. Avci, M. L. De Marco, C. Byun, J. Perrin, M. Scheel, C. Boissière and M. Faustini, *Adv. Mater.*, 2021, **33**, 2104450; (b) M. Odziomek, F. Thorimbert, C. Boissiere, G. L. Drisko, S. Parola, C. Sanchez and M. Faustini, *Adv. Mater.*, 2022, **34**, 2204489.

5   S. Bose, D. Sengupta, T. M. Rayder, X. Wang, K. O. Kirlikovali, A. K. Sekizkardes, T. Islamoglu and O. K. Farha, *Advanced Functional Materials*, 2023, 2307478.

6   (a)   Z. Zhao, X. Li, S. Huang, Q. Xia and Z. Li, *Industrial & Engineering Chemistry Research*, 2011, **50**, 2254; (b)   K. Yanagita, J. Hwang, J. A. Shamim, W.-L. Hsu, R. Matsuda, A. Endo, J.-J. Delaunay and H. Daiguji, *The Journal of Physical Chemistry C*, 2019, **123**, 387; (c)   M. W. Logan, S. Langevin and Z. Xia, *Scientific Reports*, 2020, **10**, 1492.

7   K. I. Hadjiivanov, D. A. Panayotov, M. Y. Mihaylov, E. Z. Ivanova, K. K. Chakarova, S. M. Andonova and N. L. Drenchev, *Chemical Reviews*, 2021, **121**, 1286.

8   R. Li, M. Faustini, C. Boissiere and D. Grosso, *Journal of Physical Chemistry C*, 2014, **118**, 17710.

9   (a) C. Boissiere, D. Grosso, S. Lepoutre, L. Nicole, A. B. Bruneau and C. Sanchez, *Langmuir*, 2005, **21**, 12362; (b)   M. Boudot, D. R. Ceratti, M. Faustini, C. Boissiere and D. Grosso, *Journal of Physical Chemistry C*, 2014, **118**, 23907; (c)   H. Pasco, A. Lesaine, A. Cerasuolo, C. Boissière, P. Walter, C. Sanchez, L. de Viguerie and M. Faustini, *Advanced Materials Interfaces*, 2023, 2300563.

10   (a) T. Stassin, R. Verbeke, A. J. Cruz, S. Rodríguez-Hermida, I. Stassen, J. Marreiros, M. Krishtab, M. Dickmann, W. Egger, I. F. J. Vankelecom, S. Furukawa, D. De Vos, D. Grosso, M. Thommes and R. Ameloot, *Advanced Materials*, 2021, **33**, 2006993; (b)   A. Demessence, P. Horcajada, C. Serre, C. Boissière, D. Grosso, C. Sanchez and G. Férey, *Chemical Communications*, 2009, 7149; (c)   A. Demessence, C. Boissière, D. Grosso, P. Horcajada, C. Serre, G. Férey, G. J. A. A. Soler-Illia and C. Sanchez, *Journal of Materials Chemistry*, 2010, **20**, 7676.

11   O. Dalstein, D. R. Ceratti, C. Boissière, D. Grosso, A. Cattoni and M. Faustini, *Advanced Functional Materials*, 2016, **26**, 81.

12   N. Elgrishi, K. J. Rountree, B. D. McCarthy, E. S. Rountree, T. T. Eisenhart and J. L. Dempsey, *Journal of Chemical Education*, 2018, **95**, 197.

13   G. Férey, C. Mellot-Draznieks, C. Serre, F. Millange, J. Dutour, S. Surblé and I. Margiolaki, *Science*, 2005, **309**, 2040.

14   O. Dalstein, E. Gkaniatsou, C. Sicard, O. Sel, H. Perrot, C. Serre, C. Boissière and M. Faustini, *Angewandte Chemie International Edition*, 2017, **56**, 14011.

15   H. Amyar, C. Byun, M. Besbes, A. Cattoni, H. Amenitsch, C. Boissiere and M. Faustini, *Journal of Sol-Gel Science and Technology*, 2023, 1.

16   S. Fei, J. Gao, R. Matsuda, A. Endo, W.-L. Hsu, J.-J. Delaunay and H. Daiguji, *The Journal of Physical Chemistry C*, 2022, **126**, 15538.

17   S. Fei, A. Alizadeh, W.-L. Hsu, J.-J. Delaunay and H. Daiguji, *The Journal of Physical Chemistry C*, 2021, **125**, 26755.